Research Article

Nano Research
2022, 15(9): 8564–8572

ISSN 1998-0124 CN 11-5974/O4
https://doi.org/10.1007/s12274-022-4421-4

Size matters: Steric hindrance of precursor molecules controlling the evolution of CdSe magic-size clusters and quantum dots

Juan Shen[1], Chaoran Luan[2] (✉), Nelson Rowell[3], Yang Li[4], Meng Zhang[1], Xiaoqin Chen[4], and Kui Yu[1,2,4] (✉)

[1] *Institute of Atomic and Molecular Physics, Sichuan University, Chengdu 610065, China*
[2] *Laboratory of Ethnopharmacology, Tissue-orientated Property of Chinese Medicine Key Laboratory of Sichuan Province, West China School of Medicine, West China Hospital, Sichuan University, Chengdu 610065, China*
[3] *Metrology Research Centre, National Research Council Canada, Ottawa, Ontario K1A 0R6, Canada*
[4] *Engineering Research Center in Biomaterials, Sichuan University, Chengdu 610065, China*

Received: 14 February 2022 / **Revised:** 27 March 2022 / **Accepted:** 12 April 2022

ABSTRACT

Little is known about how to precisely promote the selective production of either colloidal semiconductor metal chalcogenide (ME), magic-size clusters (MSCs), or quantum dots (QDs). Recently, a two-pathway model has been proposed to comprehend their evolution; here, we reveal for the first time that the size of precursors plays a decisive role in the selected evolution pathway of MSCs and QDs. With the reaction of cadmium myristate ($Cd(MA)_2$) and tri-n-octylphosphine selenide (SeTOP) in 1-octadecene (ODE) as a model system, the size of Cd precursors was manipulated by the steric hindrance of carboxylic acid (RCOOH) additive. Without RCOOH, the reaction produced both CdSe MSCs and QDs (from 100 to 240 °C). With RCOOH, the reaction produced MSCs or QDs when R was small (such as CH_3−) or large (such as C_6H_5−), respectively. According to the two-pathway model, the selective evolution is attributed to the promotion and suppression of the self-assembly of Cd and Se precursors, respectively. We propose that the addition of carboxylic acid may occur ligand exchange with $Cd(MA)_2$, causing the different sizes of Cd precursor. The results suggest that the size of Cd precursors regulates the self-assemble behavior of the precursors, which dictates the directed evolution of either MSCs or QDs. The present findings bring insights into the two-pathway model, as the size of M and E precursors determine the evolution pathways of MSCs or QDs, the understanding of which is of great fundamental significance toward mechanism-enabled design and predictive synthesis of functional nanomaterials.

KEYWORDS

cadmium selenide (CdSe), magic-size clusters (MSCs), quantum dots (QDs), self-assembly, steric hindrance

1 Introduction

Controlled synthesis has been the central theme of material science and it is about selective tuning of the formation and transformation of molecules. For the production of colloidal semiconductor quantum dots (QDs), the coproduction of magic-size clusters (MSCs) has often been observed [1–4]. MSCs and QDs have different optical properties. Generally, the optical absorption and emission (if there is) bandwidth of MSCs are narrower than that of QDs, due to the tighter size distribution of MSCs [4–13]. Also, for samples extracted from a reaction batch, the absorption and emission feature of MSCs are at fixed wavelengths, while QDs exhibit relatively broad optical absorption and emission that continuously redshift due to the growth in size [3, 5, 14, 15].

The growth relationship between MSCs and QDs has not yet reached a consensus. MSCs were regarded as the nuclei [2, 4, 6] (Scheme S1 in the Electronic Supplementary Material (ESM)) or the source of monomers [16–18] (Scheme S2 in the ESM) in the formation of QDs. In previous studies, some investigations have been performed via the utilization of additives in a reaction to synthesize MSCs [19–26] or QDs [27–32] (Table S1 in the ESM). For binary II-VI metal chalcogenide (ME), in a reaction batch with cadmium myristic ($Cd(MA)_2$) as Cd source, it was claimed that the addition of acetic acid (EA) promoted the formation of CdSe MSCs [26]. In addition, trimethylpentylphosphinic acid (TMPPA) was used as the ligand of Cd cation to synthesize CdSe QDs. Numerous synthetic researches have been documented that involved a laborious trial-and-error scheme to produce QDs and MSCs. However, until now, how the acid precisely controls the selective production of MSCs or QDs is still unknown.

A two-pathway model was proposed to explain the evolution of MSCs and QDs [33–35]. For Pathway 1, self-assembly of cation and anion precursors first occurs, followed by the bonding between them to form the precursor compounds (PCs). Then PCs could transform to MSCs via an intramolecular re-organization [36–41]. For the other Pathway 2, without self-assembly, the bonding of cation and anion precursors results in the formation of monomers (Mo) and fragments (Fr), which leads to the nucleation and growth of QDs followed the conventional LaMer model of classical nucleation theory [42–45]. Pathways 1 and 2 are linked by the PCs, which was commonly observed as the transition from MSCs to QDs [46]. We highlight the value and utility of the PCs with the related self-assembly produced via Pathway 1 to respond the question of "How Far Can We Push

Address correspondence to Chaoran Luan, luanc@scu.edu.cn; Kui Yu, kuiyu@scu.edu.cn

Chemical Self-Assembly?" [47]. While the two-pathway model has been proposed to theoretically understand the evolution of MSCs and QDs, it is unclear how these two pathways are experimentally controlled.

In this work, we report a study on how to control the synthesis of QDs or MSCs, using CdSe as a model system. CdSe MSCs and QDs were selectively synthesized via tuning the size of Cd precursor, which was manipulated by the addition of acids with different steric hindrance (Scheme 1). Here, steric hindrance is used to designate the space required for the alkyl and aryl group in the α-position of carboxylic acids, while "small" or "large" are used to describe the relative steric hindrance of acid additives comparing to the origin capping ligand myristic acid (MA). The acids used as additives are summarized in Table 1, with the abbreviations used in the present study. For the reaction batch without acid addition, MSCs and QDs are simultaneously present (Fig. 1(a)). While the addition of relatively small steric hindrance acid (such as EA) and relatively large steric hindrance acid (such as phenylformic acid (PhA)) results in the evolution of single ensemble of MSCs and QDs, respectively (Figs. 1(b) and 1(c)). We found that CdSe MSCs evolved when relatively small steric hindrance acids are used. And the quantity of CdSe MSC-393 produced seems to be related to the chain length of acid (Fig. 2). On the contrary, the acid with large steric hindrance favors the formation of QDs, only when the amount added is relatively large (Fig. 3). Figure 4 presents a ^{1}H and ^{13}C nuclear magnetic resonance (NMR) spectroscopy study to comprehend the formation of MSCs or QDs. The results support our speculation that ligand exchange ability is regulated by steric hindrance of acids. We validate further after the formation of MSCs, the transformation of MSCs to QDs is promoted by adding large steric hindrance acid (Fig. 5). This study introduces the concept of steric hindrance of ligands, which precisely controls the selective production of MSCs and QDs. A latest perspective mentioned that "the exact role of ligands on the formation and stabilization of MSCs remains unclear" [48]. Here we propose that the ligand exchange occurs with different steric hindrance acid additives, which regulates the size of precursors, thereby tunning formation and stabilization of MSCs/QDs. The proposed production controlling method enlightens our understanding on the self-assembly behavior of the precursors in the induction period of QDs, and brings a deeper insight in the two-pathway model, which benefits the mechanism-enabled design and predictive synthesis of functional nanomaterials.

2 Experimental

2.1 Chemicals

All chemicals, including cadmium oxide (CdO, 99.99%), 1-octadecene (ODE, $C_{18}H_{36}$, 90.0%), tri-noctylphosphine (TOP, 90.0%), butyric acid (BA, ≥ 99%), and myristic acid (MA, $C_{13}H_{27}COOH$, ≥ 99.0%) were purchased from Sigma-Aldrich. Selenium powder (Se, 99.99%, Alfa Aesar), toluene (Tol, 99.5%), EA (AR), propionic acid (PA, AR), and methanol (99.5%) were purchased from Chendu Kelong. 2-methylpropionic acid (MPA, 99%), cyclopentanecarboxylic acid (CA, 98%+), 2-methylbutyric acid (MBA, 99%), 2-phenylpropionic acid (MPhEA, 98%), and PhA (99%) were purchased from damas-beta. Cyclopentylacetic acid (CEA, > 98%) was purchased from tumor growth inhibition (TGI). 2-Phenylbutyric acid (EPhEA) was purchased from Vetec. All chemicals were commercially available and were used as received.

2.2 Synthesis of precursors

2.2.1 *Synthesis of $Cd(MA)_2$ stock solution*

For the $Cd(MA)_2$ stock solution, CdO (1.0272 g, 4.00 mmol), MA (4.0194 g, 8.80 mmol), and ODE (34.9534 g) were added to a 250 mL three-necked flask. The mixture was degassed three times and was stirred under vacuum at room temperature for 30 min until no bubbles were observed. Then the mixture was heated up to 120 °C under a N_2 atmosphere; the mixture was evacuated and then purged with N_2 at room temperature; this procedure was repeated three times until no bubbles were observed under vacuum. Then the reaction temperature was increased to 240 °C under a N_2 atmosphere thus forming a transparent and colorless solution. The mixture was then cooled to 120 °C under vacuum for another 2 h before it was cooled to room temperature under N_2 for storage.

2.2.2 *Synthesis of SeTOP*

For the SeTOP solution, Se powder (0.0118 g, 0.15 mmol) was loaded in a 4 mL sample vial, then transferred into the glove box. TOP (0.2220 g, 0.60 mmol) was injected into the vial, after which the mixture was removed from the glovebox. The mixture was stirred at room temperature. When the Se power had dissolved in the TOP completely, the solution became transparent and colorless.

2.3 Synthesis of CdSe MSCs or QDs

For a typical CdSe batch, $Cd(MA)_2$ stock solution (3.0000 g, 0.60 mmol) and ODE (1.7662 g) were added to a 50 mL three-necked round-bottom flask equipped with a condenser. The total weight of the reaction mixture was 5.0000 g. The mixture was degassed at room temperature for 30 min, at which time bubbles were no longer present. Under N_2, the temperature was increased to 70 °C, then the mixture was evacuated and then purged with N_2; this procedure was repeated three times in 10 min until no bubbles were observed under vacuum. The reaction mixture was then heated to 100 °C under N_2, and placed under vacuumed for 20 min, then cycled three times in 10 min between N_2 atmosphere and vacuum. Under a N_2 atmosphere, SeTOP fresh solution (0.2338 g, 0.15 mmol Se) was added. The reaction temperature was increased to 240 °C in a step of 20 °C. Samples were extracted after 15 min had elapsed at each temperature. For the batches with acid addition, acids were added just before SeTOP. And the amount of ODE was adjusted to keep the total weight of 5.0000 g.

2.4 Characterization

The ultraviolet–visible (UV–vis) absorption spectra were collected on a Hitachi UH4150 spectrometer with a 0.5 or 1 nm interval (between 300 and 700 nm). The quartz cuvettes (3.5 mL standard QS cells with the light path of 10 mm) were purchased from Hellma Analytics. Usually, it required about ~ 1 min to prepare the dispersions prior to the absorption data collection. Photoluminescence spectra were collected between 360 and 690 nm on a Horiba Fluoromax-4 spectrometer with an excitation wavelength of 350 nm. The slit width for both absorption and emission was 2.5 nm. To prepare a dispersion for measurement, a volume of 15 μL of the as-synthesized sample was dispersed in 3.0 mL of Tol.

For the transmission electron microscopy (TEM) measurements, 5.0 g MSC sample was purified with 2 mL Tol and 1 mL MeOH, followed by centrifuging (9,000 rpm for 3 min); this operation was repeated another two times. For the QDs, 5.0 g sample was purified with Na_2CO_3 (aq), which was dropwise added until the solution was neutral to remove excess PhA, while the ODE remained; then the solution was centrifuged (9,000 rpm for

3 min). The precipitates were dried and stored at room temperature. The samples were dispersed in Tol and dripped on a cooper grid, which was placed in a fume-hood for solvent evaporation. The images were taken on FEI Tecnai G2 F20 S-TWIN and JEM-2100 Plus (Sichuan University).

For the X-ray diffraction (XRD) measurements, the MSC sample was purified with same method in TEM study, but with 3.0 mL Tol. The purified QD sample was obtained as that in TEM study. The precipitates were under vacuum (–0.1 MPa) overnight at room temperature for XRD. The XRD patterns were collected on a Shimadzu X-ray diffractometer 6100 with Cu Kα radiation (λ = 1.5406 Å). The data were collected in a θ–θ mode between 10° and 80° at the rate of 2° per minute.

For the sample preparation of NMR measurements, 3.0000 g $Cd(MA)_2$ (0.60 mmol) and ODE (the amount was adjusted to keep the total weight of 4.7662 g) were mixed at room temperature. When the temperature was 100 °C, 0.2882 (4.80 mmol) or 0.0721 g (1.20 mmol) EA was added; the temperature was raised to 120 °C and kept for 15 min. The products were purified with 3 mL Tol, followed by centrifuging (9,000 rpm for 3 min); after the removal of supernatant, this operation was repeated three times. The samples with PhA were obtained with similar method, but with 0.5862 g (4.80 mmol) or 0.1465 g (1.20 mmol) PhA added. The product was purified with Na_2CO_3 (aq), which was dropwise added until the solution was neutral to remove excess PhA, while the ODE remained. These white precipitates were stored and dried at room temperature. The samples of EA and PhA were used as received. Then these samples were dispersed in dimethyl sulfoxide-d6 (DMSO-d_6, 600 μL) for NMR analyzing. The ^{1}H NMR signal was corrected with DMSO characteristic resonance signal (2.51 ppm) as a reference, and the correction of ^{13}C NMR was also referred by DMSO (39.52 ppm). The samples were measured at room temperature at Bruker A II 400 Mhz NMR apparatus. The assignment was assisted by MestReNova software.

Fourier transform infrared spectroscopy (FTIR) measurements were conducted on a Bruker Tensor 27 FTIR spectrometer using KBr pellets. The samples of $Cd(MA)_2$ + EA/PhA were obtained as in NMR study. And 3.0 g stock solution $Cd(MA)_2$ was added in 3 mL Tol and centrifuged (9,000 rpm for 3 min); after the removal of supernatant, the operation was repeated another two times. The samples d and e were purchased without purification. Each sample (1–2 mg) and KBr (200 mg) were taken in an agate mortar for grinding and mixing under infrared light. The mixed sample was pressed to be translucent for measurement.

3 Results and discussion

We used CdSe as the model to study the selective production of either MSCs or QDs. For a reaction of $Cd(MA)_2$ and SeTOP in ODE, while acid additive was added at 100 °C before SeTOP. The temperature of reaction batches was then increased from 100 to 240 °C in steps of 20 °C. For all the reaction batches, the feed molar ratio of $Cd(MA)_2$ (0.60 mmol) to Se (0.15 mmol) was fixed at 4 to 1, with a Se concentration of 30 mmol·kg^{-1} and a total weight of the reaction mixture of 5.0000 g.

3.1 The selective production of QDs and MSCs via adding acid with different steric hindrance

In Fig. 1, we present the optical absorption and emission spectra extracted from three as-synthesized CdSe batches. For batch a, SeTOP was added in the mixture of $Cd(MA)_2$ and ODE at 100 °C. For other two batches, 4.8 mmol EA (b) or PhA (c) was added before the addition of SeTOP at 100 °C. Then the reaction batches were heated to 240 °C, with an interval of 20 °C and kept at each temperature for 15 min. An aqueous (15 μL) of each sample was extracted and dispersed in 3 mL Tol for the spectral study. Results of the samples extracted at 140 °C /15 min, 160 °C /15 min, and 180 °C /15 min are shown in Fig. 1.

As shown in Fig. 1, for the samples of batch a, two characteristic absorption doublets at 373/393 and 433/460 nm were observed, which indicated the formation of CdSe MSC-393 and MSC-460. These two types of MSCs with absorption doublets have been widely reported [5, 49–52] and have been characterized by synchrotron-based small-angle X-ray scattering (SAXS), which indicated that both dMSC-393 and dMSC-460 were disc-shaped [53]. And the former can be converted to the latter with the monomer addition. A broad peak was also observed, which means both MSCs and QDs were presented when acid was not added. Furthermore, the absorbance of MSC-393 increased up to 160 °C then decreased, along with the continuous increase of MSC-460; at the same time, the absorption and emission peaks of QDs (excited

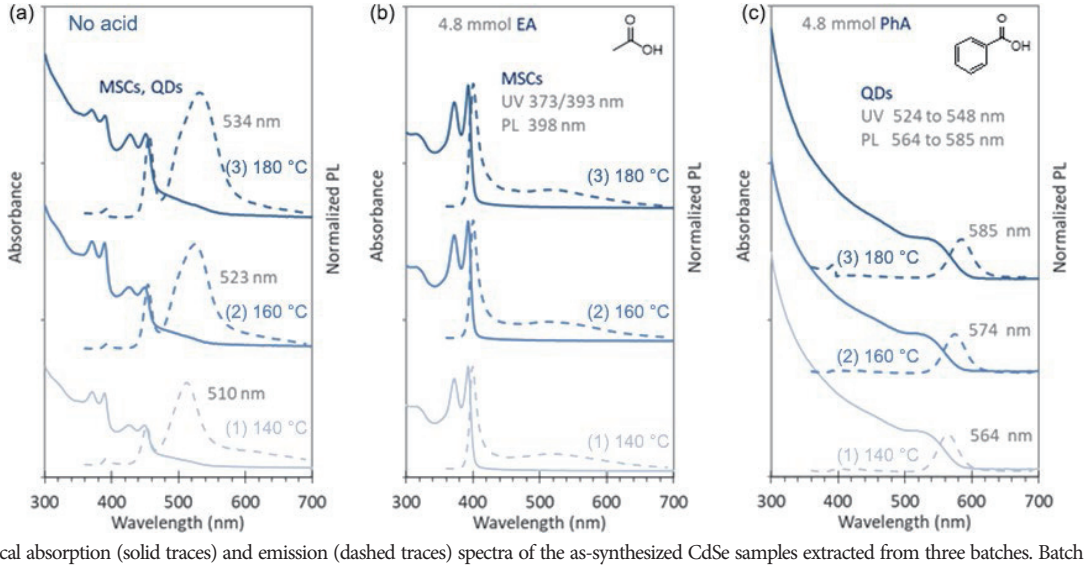

Figure 1 Optical absorption (solid traces) and emission (dashed traces) spectra of the as-synthesized CdSe samples extracted from three batches. Batch (a) dealt with the background reaction of $Cd(MA)_2$ (2.4 mmol) and SeTOP (0.6 mmol). For the Batch (b) and (c) reactions, respectively, 4.8 mmol of EA (b) or PhA (c) was added. For the spectroscopy study, an aliquot (15 μL) of each sample extracted at 140 (1), 160 (2), and 180 °C (3) was dispersed in 3.0 mL Tol. For Batch (a), both MSCs and QDs developed. For Batch (b), only MSCs evolved. For Batch (c), only QDs were observed. The acid used in Batch (b) and (c) with relatively small and large steric hindrance, respectively, promotes and suppresses the precursor self-assembly (Scheme 1); thus, the MSCs (b) and QDs (c) are produced selectively.

at 350 nm) redshifted from 493 to 522 nm and from 510 to 534 nm, respectively. For batch b samples, a characteristic absorption doublet at 373/393 nm was observed in the spectra of the samples from 140 to 180 °C. Samples of this batch exhibited sharp band edge photoluminescence (PL) peaking at 398 nm, together with broad trap emission peaking at 520 nm. Together, the optical absorption and PL spectra indicated the formation of CdSe MSC-393 with the addition of EA. In batch c, a broad peak at 526 nm was observed at 140 °C/15 min, which redshifted to 548 nm at 180 °C/15 min. The broad peak with redshift pattern is regarded as the bandgap absorption of the QDs [54]. The corresponding PL peak redshifted from 564 to 585 nm. This observation indicated QDs had nucleation and growth with adding PhA. Figure S1 in the ESM presented the complete evolution of the optical absorption properties of the samples from Fig. 1. The sample-to-sample comparison was displayed in Fig. S2 in the ESM, which showed that distinctly different products were obtained with different acids. Figure S3 in the ESM showed the TEM and XRD images of the 180 °C/15 min samples from another identical batch b and c in Fig. 1 without any sampling. Before purification, as-synthesized MSC-393 (a1) and QDs (b1) had a 0-dimension, dot-like shape, with the latter having an apparent larger size. After purification, a 2-dimension structure was observed in MSC sample (a2), while the QDs retained their size and shape (b2). The self-assembly behavior of MSCs during purification was previously reported, which led to nanoplatelet or nanohelical structure [55, 56]. MA was used as acid addition and also played the role on origin Cd precursor in the batch, as shown in Fig. S4 in the ESM. MSCs and QDs were observed together, as the batch without acid addition (Fig. 1(a) and S1(a) in the ESM). The addition of MA did not result in the selective production of MSCs or QDs.

3.2 The acid added with small steric hindrance

It is reported that the addition of small molecular acid EA and derivative ($Zn(OAc)_2$) benefits the production of MSCs [26]. In the present study, it was found that 4.8 mmol EA added in the pre-nucleation stage promoted the formation of CdSe MSC-393 and suppressed the nucleation and growth of QDs, whereas adding PhA had the opposite effect. EA and PhA are carboxylic acids with different alkyl chains. We speculated that the different size of substituent group caused different steric hindrance of acid. In this way, we can infer that the acid with larger steric hindrance inhibited self-assembly and resulted in the nucleation and growth of QDs [57]. On the contrary, acids with small steric hindrance promoted the self-assembly, causing the formation of MSCs.

To further test our hypothesis, we employed various types of acids with small steric hindrance. Figure 2 showed the amount of MSC-393 produced from six reaction batches with acid of 1.2 mmol (a) or 4.8 mmol (b) $CH_3(CH_2)_nCOOH$ (n = 0, gray bars, EA; n = 1, blue bars, PA; and n = 2, orange bars, BA). Results for the samples from 100 to 200 °C are presented in Fig. 2. The complete spectral evolution of the three batches is shown in Figs. S1(a), S5, and S6 in the ESM.

As shown in Figs. 2(a) and 2(b), the absorbance of MSC-393 increased from 100 to 180 °C with the addition of EA or PA. With the addition of BA, the absorbance of MSC-393 increased from 140 to 160 °C. When the temperature increased to 180 °C, tiny peak of CdSe MSC-460 was observed in the sample with 4.8 mmol BA added (Fig. S6(c) in the ESM); The maximum absorbance of MSC-393 was observed in the sample with EA (n = 0); while the minimum one was with BA (n = 2). Figure S7 in the ESM showed the sample-to-sample comparison of the absorbance of CdSe MSC-393 with the addition of 1.2 mmol EA, PA, and BA (the whole evolution was presented in Fig. S6 in the ESM) at different temperatures. We found that the amount of MSC-393 obtained

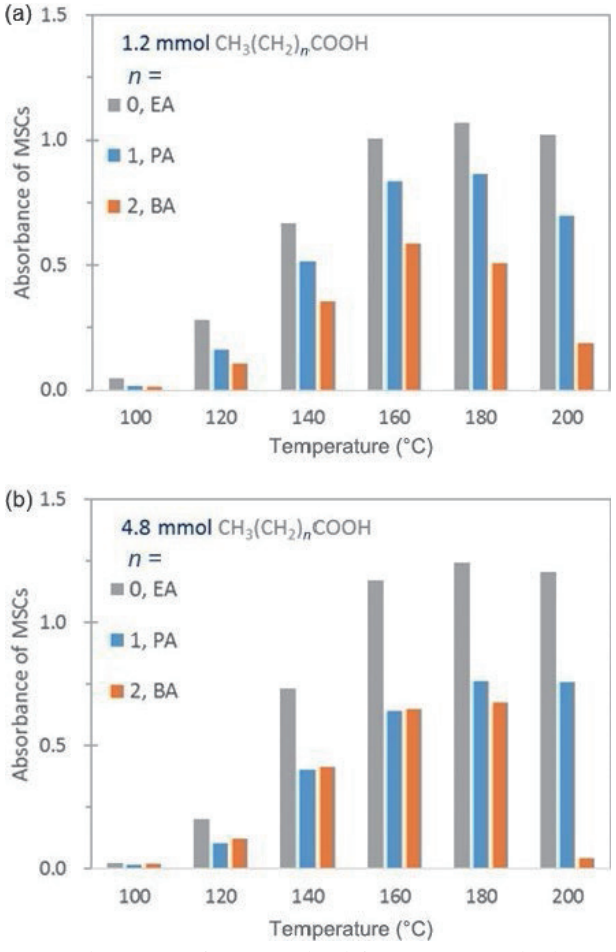

Figure 2 The amount of MSCs produced from six reactions batches with 1.2 mmol (a) or 4.8 mmol (b) acids with small steric hindrance. Three types of acids with different alkyl chain length, $CH_3(CH_2)_nCOOH$ (n = 0, 1, and 2), were added. Each sample (15 μL) was dispersed in 3.0 mL of Tol. With the increase of temperature to 180 °C, the absorbance of MSCs increased to maximum. The yield of MSCs is apparently regulated by the length of the alkyl chain. The smaller the acid steric hindrance is, the more MSCs is produced.

decreased with the increase of chain length of carboxylic acid. This result is consistent with our previous observation, that ligand with shorter chain length favors the formation of MSCs with smaller size [58].

As we have postulated, acids with small steric hindrance (such as EA, PA, and BA) benefit the formation of MSCs. Among the three acids with small steric hindrance, EA has the least while BA the most steric hindrance. As a result, the smaller the steric hindrance the acid, the greater the amount of CdSe MSCs produced. According to the two-pathway model, MSCs evolve from PCs, formation of which involves precursors self-assembly and further bonding. Here we establish that the acid with small steric hindrance facilitates the formation of MSCs, due to the ability of acid to accelerate the precursors self-assembly. In the case of micelles, the process proceeds quite differently than in the present system studied. During the formation of micelles, it is established that greater the hydrocarbon chain length of the surfactant, greater is the self-assembly formation [59]. By that analogy, we conclude that the smaller steric hindrance, the greater self-assembly.

3.3 The acid added with large steric hindrance

To better understand the effect of acids with large steric hindrance, MPA and MBA were used, in consideration of their steric hindrance resulted from the methyl on the α-position. Figure 3 presented the evolution of the optical properties of as-

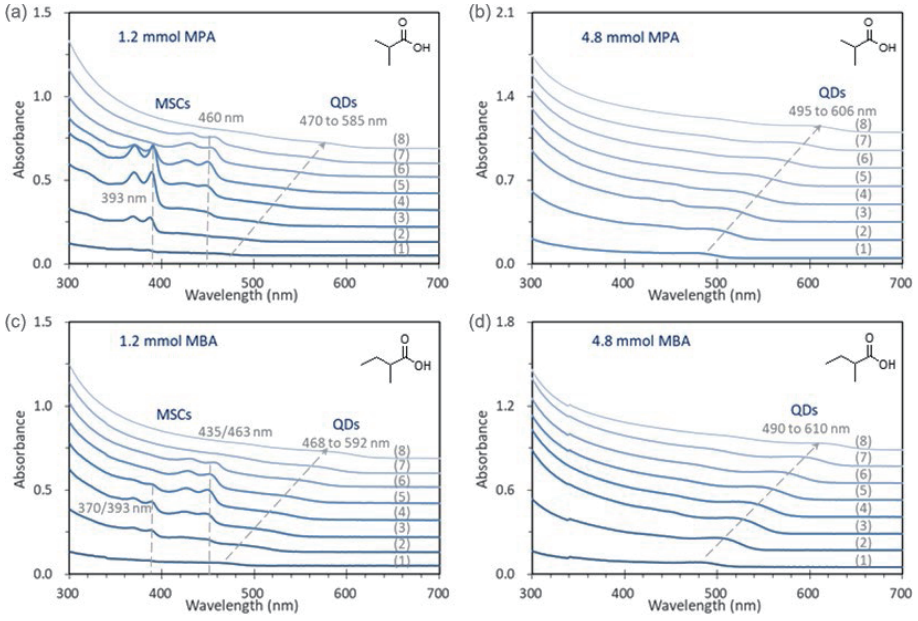

Figure 3 Evolution of optical absorption spectra (offset) of the samples extracted from 4 batches. Acids of 1.2 mmol MPA (a) or MBA (c), 4.8 mmol MPA (b) or MBA (d) was added. An aliquot (15 μL) of each sample extracted was dispersed in 3.0 mL Tol for the absorption measurement. With the addition of 1.2 mmol MPA (a), the evolution of MSCs and QDs were observed during the heating process. When the amount of MPA increased to 4.8 mmol (b), only QDs appeared. When 1.2 mmol MBA was used (c), MSCs and QDs evolved in the batch. With a larger MBA amount such as 4.8 mmol (d), only QDs produced in the reaction. Therefore, a large amount of large steric hindrance acid promotes the growth of QDs; while with small amount of these acids, MSCs and QDs coexist.

synthesized CdSe samples extracted from four batches, in which acid addition of 1.2 mmol MPA (a) or MBA (c), 4.8 mmol MPA (b) or MBA (d) was used. For each batch, eight samples were extracted at 100 °C/15 min (1), 120 °C/15 min (2), 140 °C/15 min (3), 160 °C/15 min (4), 180 °C/15 min (5), 200 °C/15 min (6), 220 °C/15 min (7), and 240 °C/15 min (8).

In Fig. 3(a), with the addition of 1.2 mmol MPA, MSCs and QDs formed at 100 °C (trace 1). The absorbance of MSC-393 increased when the temperature increased to 140 °C (trace 3). As the reaction progressed, the decrease of MSC-393 was accompanied with the increase of MSC-460 when the temperature increased from 160 (trace 4) to 200 °C (trace 6). When the temperature increased to 240 °C (trace 8), MSCs disappeared completely. At the same time, from 100 to 240 °C (traces 1 to 8), the absorption peak of QDs was also observed, which continuously redshifted from 470 to 585 nm. In Fig. 3(b), with 4.8 mmol MPA, QDs were produced, and the absorption peak of which redshifted from 495 to 606 nm. With MBA instead of MPA, as shown in Figs. 3(c) and 3(d), respectively, the samples displayed similar evolution patterns. With 1.2 mmol MBA, MSCs and QDs were both present. The absorption peak of MSC-393 was observed from 100 to 160 °C/15 min, and the absorption peak of MSC-460 evolved from 120 to 200 °C/15 min; while the peak of QDs redshifted from 468 to 592 nm. With the addition of 4.8 mmol MBA, only nucleation and growth of QDs was observed, the peak of which redshifted from 490 to 610 nm. The corresponding emission peaks are shown in Fig. S8 in the ESM.

These results revealed that different from the acids with small steric hindrance, acids with large steric hindrance favor the formation of QDs when the acid amount is relatively large. For MPA and MBA, the sample-to-sample comparison is shown in Fig. S9 in the ESM. The peak position of the samples in the MBA batch (dark blue traces) is a little larger than those in MPA batch (light blue traces).

It is worth noting that in the case of small steric hindrance acids, the addition amount influenced the yield, but not influenced the species (Fig. 2).

While for the acids with larger steric hindrance, changing the amount of acid resulted in different species (Fig. 3). With larger amount, only QDs generated. But with smaller amount, QDs and MSCs coexisted, similar to the batch without acid addition (Fig. 1(a) and Fig. S1 in the ESM). We infer that the effect of acid addition relies on the ligand exchange of the Cd precursor, which was reported in the formation of CdTe MSC-427 [23]. For acids with small steric hindrance, ligand exchange occurs with smaller amount. However, for acids with large steric hindrance, a large amount, such as 4.8 mmol, is required for ligand exchange. The quality of ligand exchange for acids is associated with their complexation ability to Cd atom. Compared to the original ligand MA, acid with larger steric hindrance has weaker ligand complexing ability; thus, a relative high concentration is required for ligand exchange. To support the inference, the spectra extracted from reaction batches with the co-addition of PA and MPA are presented in Fig. S10 in the ESM. When the amounts of PA and MPA are the same (a and b), MSCs were observed, which was the effect of small steric hindrance acid, PA. When the amount of MPA was larger (c and d), the role of MPA became more significant, which caused the production of QDs.

CA and CEA were also used as acids with large steric hindrance for their cyclopentyl group. The results in Fig. S11 in the ESM displayed a familiar trend, that with only larger amount, the acid with large steric hindrance promoted QDs. Compared to CA (a and b), CEA (c and d) had smaller steric hindrance, due to the longer alkyl chain between cyclopentyl and carboxy groups. As a result, no matter whether the batches produced MSCs and QDs (a and c), or only QDs (b and d), the QDs produced with CA had longer wavelength. We also investigated acids containing phenyl group, which led to a similar conclusion. As shown in Fig. S12 in the ESM, MPhEA (a and b) had smaller steric hindrance than EPhEA (c and d). It is apparent that QDs produced with MPhEA were smaller than those with EPhEA. The TEM images of synthesized QDs assisted by acids with different steric hindrances are presented in Fig. S13 in the ESM. The size of these QDs (the absorption peaking in the range of 522 to 548 nm) was difficult to distinguish with TEM.

It should be point out that in previous study [60], we have

demonstrated that the co-addition of diphenylphosphine ($HPPh_2$) and MBA in CdS reaction batch promoted the yield of MSCs and suppressed the nucleation and growth of QDs. What's more, with the addition of 2,2-dimethylbutyric acid, CdS QDs evolved with MSCs at 100 °C. We speculate the possible reason is that S atom is smaller than Se atom. Thus, the steric hindrance of MBA barely influenced the self-assembly behavior of those precursors. For the generation of CdS QDs, acid addition with larger steric hindrance, such as 2,2-dimethylbutyric acid, is required.

3.4 ^{1}H and ^{13}C NMR study of the ligand exchange

NMR was used to investigate our speculation regarding the relative efficacy of the ligand exchange. The detected ^{1}H and ^{13}C NMR signals of 4 samples are partially presented in Fig. 4 (whole results are present in Fig. S14 in the ESM). For samples a2, b2, a4, and b4, the batches were heated at 120 °C for 15 min after 4.8 mmol EA and PhA, respectively, was added. Then 4 spectra were collected in DMSO-d_6 at room temperature from 4 samples, which are presented in the following order: EA (purchased, trace a1 and b1),

As shown in Fig. 4, for trace a1 and b1, the signal of proton and the carbon atom of the methyl (–CH_3) of EA were observed at 1.91 and 21.48 ppm (a), respectively. For trace a2 and b2, the signal of protons and the carbon atom of the methyl (–CH_3) were appeared at 1.83 and 22.10 ppm (a'). We found that the ^{1}H resonance signal of EA exhibited an appreciable upfield shift and ^{13}C NMR signal shifted downfield. The proton signal for 1.26 ppm (b) is the characteristic absorption of methylene (–CH_2–) of MA. The phenyl (C_6H_5–) of PhA has three hydrogens and exhibits ^{1}H resonance signals (trace a3) at 7.51 ppm (b), 7.63 ppm (a), and 7.94 ppm (c), respectively, and with four carbons displayed 13C resonance signals (trace b3) at 129.0 ppm (b), 129.7 ppm (c), 131.2 ppm (d), and 133.4 (a) ppm. While for traces a4 and b4, the proton signals at 7.96, 7.49, 7.42 ppm and the carbon signals at 132.80, 132.48, 128.73, 128.47 ppm show the hydrogens and carbons of phenyl (C_6H_5–) on PhA. We observed that the ^{1}H resonance signal shifted upfield and the ^{13}C resonance signals also shifted. The chemical shift changes of EA and PhA suggested that ligand exchange occurred after the acid addition and heating, which was also supported by the FTIR results in Fig. S16 in the ESM. We also analyzed the ligands comprising these two purified samples. For sample 2, the MA to EA ratio was 1:9 (the specific quantification process is shown in Fig. S17 in the ESM). For sample 4, the MA to PhA was 1:3. The results supported our speculation that the steric hindrance of the acid influences the ligand exchange ability. The larger the steric hindrance of the acid, the less MA was replaced. When less acids were used as shown in Fig. S15 in the ESM, the resulting MA/EA and MA/PhA ratios were 1:5 and 1:3, respectively. Figure S18 in the ESM presents the visual observation of Cd precursors with different acids, which is also in agreement with our speculation of ligand exchange.

Importantly, the ^{1}H and ^{13}C resonance signals detected in the trace 2 suggest the interaction between $Cd(MA)_2$ and EA, together with the probable presence of complex of 1 eq Cd(MA)(EA) and 4 eq $Cd(EA)_2$. This indicates that an interaction between Cd(MA)2 and PhA had also occurred, and a probable formation of 1 eq Cd(MA)(PhA) and 1 eq $Cd(PhA)_2$. The substitution pattern is similar to that seen in our previous studies [23, 61]. From the data, it is reasonable to infer that these reactions occurred through ligand exchange, and the larger steric hindrance of the acid, the harder the replacement of MA is. Figure S14 in the ESM showed similar results to the Fig. 4 but with another feed molar ratio. Also, we studied the FTIR of these samples which were displayed in Fig. S16 in the ESM. Figure S18 in the ESM presented a different state of Cd precursor with the different steric hindrance acids. It shows that the addition of acid substitutes the

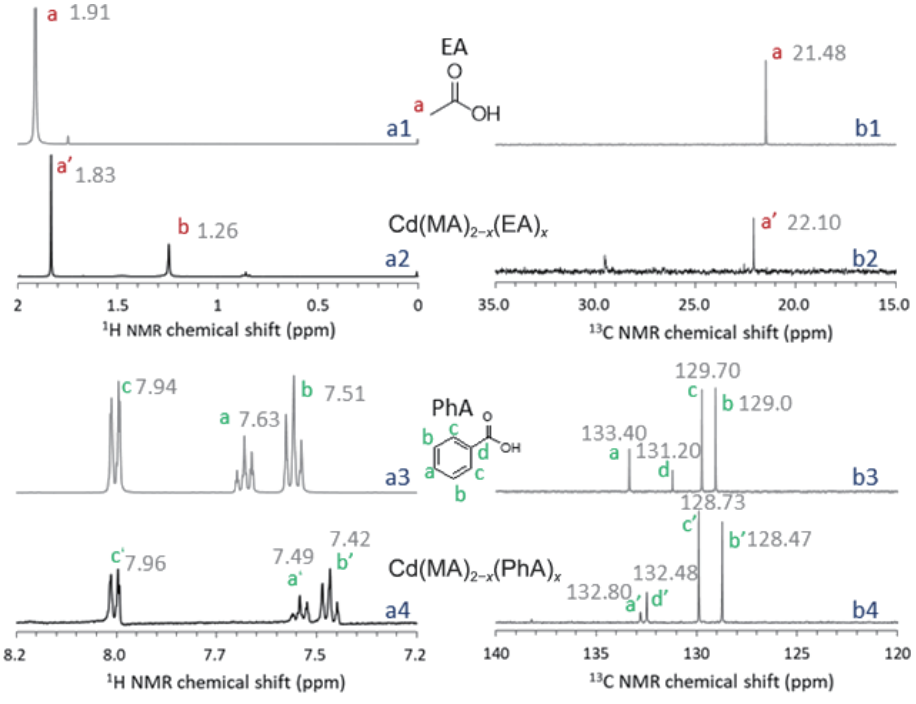

Figure 4 ^{1}H (left, a) and ^{13}C NMR (right, b) exploration of EA (purchased, trace a1 and b1), $4Cd(MA)_2$/32EA (trace a2 and b2, purified) PhA (purchased, trace a3 and b3) and $4Cd(MA)_2$/32PhA (trace a4 and b4, purified) in dimethyl DMSO-$d_6$at room temperature. Trace a2, b2, a4, and b4 are white precipitate obtain at 120 °C / 15 min after the addition of 4.8 mmol EA and PhA to a $Cd(MA)_2$ solution in ODE at 100 °C. The samples were measured at room temperature at Bruker A II 400 Mhz. Figure S14 in the ESM presents the complete NMR spectra of the a1–a4 and b1–b4. Comparing trace a1, b1 with trace a2, b2, the methyl group shifted upfield in ^{1}H NMR and downfield in ^{13}C NMR in the reaction, and the products probably were 1 eq Cd(MA)(EA) and 4 eq $Cd(EA)_2$. For trace a3, a4, b3, and b4 the phenyl group exhibited upfield shift in NMR spectra, and the equal proportions Cd(MA)(PhA) and $Cd(PhA)_2$ were obtained. Evidently, the interaction between $Cd(MA)_2$ and EA or PhA occurred. $4Cd(MA)_2$/32EA (purified, trace a2 and b2), PhA (purchased, trace a3 and b3) and $4Cd(MA)_2$/32PhA (purified, trace a4 and b4). For another two samples with 1.2 mmol EA and PhA obtained with a similar process, the NMR results were presented in Fig. S15 in the ESM.

MA ligand on Cd atom. The smaller the acid steric hindrance, the more self-assembly process happens [62]. Such a ligand substitution behavior should be suit for various reaction systems. For example, for a reaction batch with PhA as origin capping ligand, it is reasonable to predict that QDs should be the products. While the additive of EA or MA should result in the production of MSCs or the mixture of MSCs and QDs, respectively.

3.5 The acid added at different stages

After having discussed the effect of the acid addition on self-assembly before Cd–Se bonding, we now examine the effect of acid when added after the formation of MSCs. Figure 5 displayed the evolution of optical absorption (solid traces) and PL (dashed traces) spectra collected from samples extracted from one batch. In batch a, 1.2 mmol PA was added at 100 °C followed by SeTOP, and then the temperature was increased to 160 °C, with an interval of 20 °C and a reaction period of 15 min at each temperature. When the temperature reached to 180 °C/0 min, 4.8 mmol MPA was immediately added into the reaction. We continued to increase the temperature to 240 °C in steps of 20 °C, holding at each temperature for 15 min.

As shown in Fig. 5(a), with 1.2 mmol PA added, CdSe MSC-393 evolved without the nucleation and growth of QDs. The corresponding emission peaks exhibited one sharp emission at 398 m with broad trap emission at 538 nm. After 4.8 mmol MPA added at 180 °C/0 min, as shown in Fig. 5(b), CdSe MSC-393 disappeared completely, while a broad peak at 580 nm was observed at 180 °C, which redshifted to 615 nm at 240 °C. For the emission, the peak redshifted from 585 to 625 nm. When PA was added, MSCs evolved and increased with temperature changes, while after the addition of MPA, QDs produced at the cost of the MSCs produced. Such results are consistent with the reported two-pathway model [33–35,46]. To clarify whether the QDs were produced from the addition of MPA, or from the temperature increase, another batch was prepared for which the results appeared in Fig. S19 in the ESM. Four samples were extracted, after the addition of 4.8 mmol of MPA with the temperature held at 180 °C for 20 min. In this case when the MPA was added, decrease of MSC-393 and formation of QDs were observed at 180 °C. Furthermore, when the amount of MPA added at 180 °C/0 min was decreased to 1.2 mmol (Fig. S20 in the ESM), only some of the MSCs were converted into QDs. Similar results were observed in the batches with various acids, including a batch when 4.8 mmol of MBA was added in the reaction with 1.2 mmol BA (Fig. S21 in the ESM), a batch when 4.8 mmol of MPA was added in the reaction with 1.2 mmol MPA (Fig. S22 in the ESM), and a batch when 4.8 mmol of MBA was added in the reaction with 1.2 mmol MBA (Fig. S23 in the ESM).

We can still use ligand steric hindrance to explain the changes from MSCs to QDs. For each batch, after the acid was added at 180 °C, ligand exchange occurred. The resulting MSC/PC with large steric hindrance ligand was unstable, which fragmentized to monomers/fragments. The formed monomers/fragments led to nucleation and growth of QDs. As a result, formation of QDs was observed, accompanied by the disappearance of MSCs. And in all the cases, large steric hindrance acids were used at the second time (180 °C) to facilitate QDs, so a larger amount was required for ligand exchange. The ligands with large steric hindrance not only inhibit precursor self-assembly and the formation of PCs, but also decompose the formed PCs. Combining these effectively promotes the nucleation and growth of QDs.

4 Conclusions

In conclusion, we have systematically studied, for the first time, the size of Cd precursors plays a decisive role in tuning the selective production of either MSCs or QDs (Scheme 1). For a reaction produces MSCs and QDs together, acid additives with different steric hindrance result in the selective synthesis of MSCs or QDs (Fig. 1). Acids with small steric hindrance result in MSCs

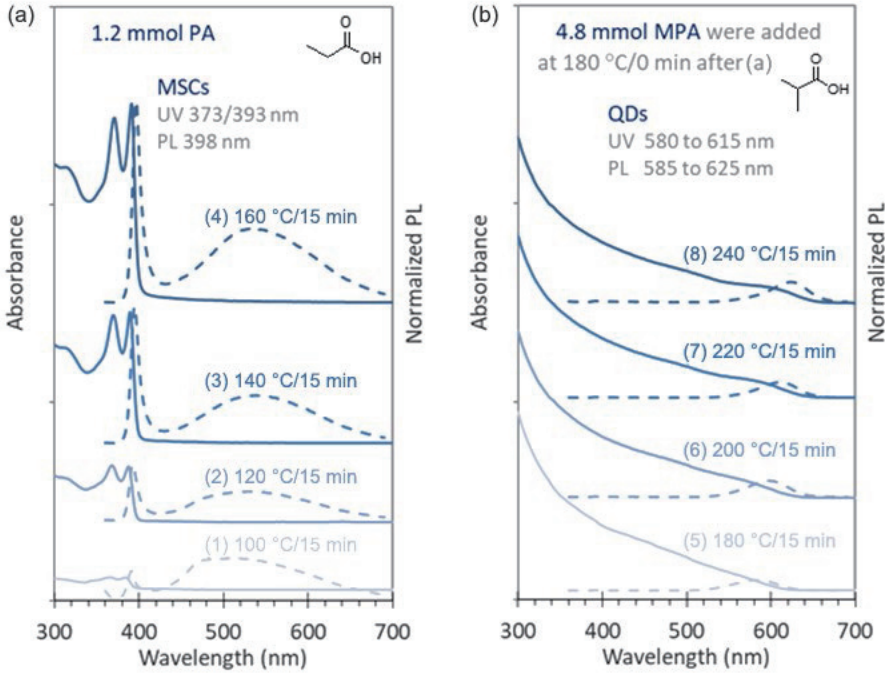

Figure 5 Evolution of optical absorption (solid traces) and PL (dashed traces) spectra collected from samples extracted from one batch with PA and MPA added at different temperature. At 100 °C, 1.2 mmol PA was added. As shown in part (a), four samples extracted after 15 min held at 100, 120, 140, and 160 °C. Then the temperature was increased to 180 °C and 4.8 mmol MPA was added to the reaction. Four other samples were extracted after 15 min held at 180, 200, 220, and 240 °C (b). An aliquot (15 μL) of each sample extracted was dispersed in 3.0 mL Tol for spectroscopy study. In batch a, with 1.2 mmol of added PA, MSCs were observed. These samples exhibited sharp emission peaks at 398 nm. When another 4.8 mmol MPA was added to the reaction at 180 °C/0 min, QDs were generated instead. The addition of MPA appears to have fragmentized the formed PC, which led to the disappearance of MSCs and the nucleation and growth of QDs.

with adjustable production yield (Fig. 2); while acids with large steric hindrance lead to QDs with tunable size (Fig. 3). NMR study (Fig. 4) reveals that ligand exchange occurs between acid additive and origin ligand MA. We propose that acid additives via ligand exchange control the size of the Cd precursor. When the size of Cd precursor is small, the self-assembly process is favored, and thus the formation of MSCs is favored; while Cd precursor with large size inhibits the self-assembly process and thus leads to the nucleation and growth of QDs. This hypothesis is further supported by the large steric hindrance acid induced MSC to QD transition (Fig. 5). The study reveals acid additives affect the size and self-assemble behavior of the precursors, which regulates the selective products of MSCs or QDs. As a supporting to the two-pathway model for the formation of MSCs and QDs, the present work further develops mechanism-directed selective syntheses of nanoparticles. Embracing the formation and transformation of molecules in synthesis can further advance materials science.

Acknowledgements

K. Y. thanks the National Natural Science Foundation of China (NSFC, No. 21773162), the Fundamental Research Funds for the Central Universities, the Applied Basic Research Programs of Science and Technology Department of Sichuan Province (No, 2020YJ0326), the State Key Laboratory of Polymer Materials Engineering of Sichuan University respectively for No. sklpme2020-2-09, and the Open Project of Key State Laboratory for Supramolecular Structures and Materials of Jilin University for No. SKLSSM 2021030. M. Z. is grateful to National Natural Science Foundation of China ((NSFC, No. 22002099), China Postdoctoral Science Foundation (No. 2020T130441), Sichuan University postdoctoral interdisciplinary Innovation Fund and the Open Project of Key State Laboratory for Supramolecular Structures and Materials of Jilin University (No. SKLSSM 2021032). C. R. L. is grateful to the COVID-19 Science and Technology Emergency Project of Sichuan Province of China (No. 2021YFS0408). We thank the Analytical & Testing Center of Sichuan University for TEM.

Electronic Supplementary Material: Supplementary material (additional optical absorption spectra, TEM, NMR, FT-IR, and XRD) is available in the online version of this article at https://doi.org/10.1007/s12274-022-4421-4.

References

[1] Bootharaju, M. S.; Baek, W.; Lee, S.; Chang, H.; Kim, J.; Hyeon, T. Magic-sized stoichiometric II–VI nanoclusters. *Small* **2021**, *17*, 2002067.

[2] Pan, D. C.; Ji, X. L.; An, L. J.; Lu, Y. F. Observation of nucleation and growth of CdS nanocrystals in a two-phase system. *Chem. Mater.* **2008**, *20*, 3560–3566.

[3] Ouyang, J. Y.; Kuijper, J.; Brot, S.; Kingston, D.; Wu, X. H.; Leek, D. M.; Hu, M. Z.; Ripmeester, J. A.; Yu, K. Photoluminescent colloidal CdS nanocrystals with high quality via noninjection one-pot synthesis in 1-octadecene. *J. Phys. Chem. C* **2009**, *113*, 7579–7593.

[4] Peng, Z. A.; Peng, X. G. Nearly monodisperse and shape-controlled CdSe nanocrystals via alternative routes: Nucleation and growth. *J. Am. Chem. Soc.* **2002**, *124*, 3343–3353.

[5] Kudera, S.; Zanella, M.; Giannini, C.; Rizzo, A.; Li, Y.; Gigli, G.; Cingolani, R.; Ciccarella, G.; Spahl, W.; Parak, W. J. et al. Sequential growth of magic-size CdSe nanocrystals. *Adv. Mater.* **2007**, *19*, 548–552.

[6] Kasuya, A.; Sivamohan, R.; Barnakov, Y. A.; Dmitruk, I. M.; Nirasawa, T.; Romanyuk, V. R.; Kumar, V.; Mamykin, S. V.; Tohji, K.; Jeyadevan, B. et al. Ultra-stable nanoparticles of CdSe revealed from mass spectrometry. *Nat. Mater.* **2004**, *3*, 99–102.

[7] Wang, R. B.; Ouyang, J. Y.; Nikolaus, S.; Brestaz, L.; Zaman, B.; Wu, X. H.; Leek, D.; Ratcliffe, C. I.; Yu, K. Single-sized colloidal CdTe nanocrystals with strong bandgap photoluminescence. *Chem. Commun.* **2009**, 962–964.

[8] Wang, Y. Y.; Zhou, Y.; Zhang, Y.; Buhro, W. E. Magic-size II–VI nanoclusters as synthons for flat colloidal nanocrystals. *Inorg. Chem.* **2015**, *54*, 1165–1177.

[9] Dukes III, A. D.; McBride, J. R.; Rosenthal, S. J. Synthesis of magic-sized CdSe and CdTe nanocrystals with diisooctylphosphinic acid. *Chem. Mater.* **2010**, *22*, 6402–6408.

[10] Hsieh, T. E.; Yang, T. W.; Hsieh, C. Y.; Huang, S. J.; Yeh, Y. Q.; Chen, C. H.; Li, E. Y.; Liu, Y. H. Unraveling the structure of magic-size $(CdSe)_{13}$ cluster pairs. *Chem. Mater.* **2018**, *30*, 5468–5477.

[11] Nevers, D. R.; Williamson, C. B.; Savitzky, B. H.; Hadar, I.; Banin, U.; Kourkoutis, L. F.; Hanrath, T.; Robinson, R. D. Mesophase formation stabilizes high-purity magic-sized clusters. *J. Am. Chem. Soc.* **2018**, *140*, 3652–3662.

[12] Mule, A. S.; Mazzotti, S.; Rossinelli, A. A.; Aellen, M.; Prins, P. T.; van der Bok, J. C.; Solari, S. F.; Glauser, Y. M.; Kumar, P. V.; Riedinger, A. et al. Unraveling the growth mechanism of magic-sized semiconductor nanocrystals. *J. Am. Chem. Soc.* **2021**, *143*, 2037–2048.

[13] Wang, P.; Yang, Q. Q.; Xu, C.; Wang, B.; Wang, H.; Zhang, J. D.; Jin, Y. D. Magic-sized CdSe nanoclusters for efficient visible-light-driven hydrogen evolution. *Nano Res.* **2022**, *15*, 3106–3113.

[14] Dagtepe, P.; Chikan, V.; Jasinski, J.; Leppert, V. J. Quantized growth of CdTe quantum dots; observation of magic-sized CdTe quantum dots. *J. Phys. Chem. C* **2007**, *111*, 14977–14983.

[15] Yu, K. CdSe magic-sized nuclei, magic-sized nanoclusters and regular nanocrystals: Monomer effects on nucleation and growth. *Adv. Mater.* **2012**, *24*, 1123–1132.

[16] Friedfeld, M. R.; Johnson, D. A.; Cossairt, B. M. Conversion of InP clusters to quantum dots. *Inorg. Chem.* **2019**, *58*, 803–810.

[17] Gary, D. C.; Terban, M. W.; Billinge, S. J. L.; Cossairt, B. M. Two-step nucleation and growth of InP quantum dots via magic-sized cluster intermediates. *Chem. Mater.* **2015**, *27*, 1432–1441.

[18] Jiang, Z. J.; Kelley, D. F. Role of magic-sized clusters in the synthesis of CdSe nanorods. *ACS Nano* **2010**, *4*, 1561–1572.

[19] Liu, X. M.; Jiang, Y.; Guo, W. M.; Lan, X. Z.; Fu, F. M.; Huang, W. Y.; Li, L. J. One-pot synthesis of CdSe magic-sized nanocrystals using selenium dioxide as the selenium source compound. *Chem. Eng. J.* **2013**, *230*, 466–474.

[20] Newton, J. C.; Ramasamy, K.; Mandal, M.; Joshi, G. K.; Kumbhar, A.; Sardar, R. Low-temperature synthesis of magic-sized CdSe nanoclusters: Influence of ligands on nanocluster growth and photophysical properties. *J. Phys. Chem. C* **2012**, *116*, 4380–4389.

[21] Ithurria, S.; Bousquet, G.; Dubertret, B. Continuous transition from 3D to 1D confinement observed during the formation of CdSe nanoplatelets. *J. Am. Chem. Soc.* **2011**, *133*, 3070–3077.

[22] Singh, S.; Tomar, R.; Brinck, S. T.; Roo, J.; Geiregat, P.; Martins, J. C.; Infante, I.; Hens, Z. Colloidal CdSe nanoplatelets, a model for surface chemistry/optoelectronic property relations in semiconductor nanocrystals. *J. Am. Chem. Soc.* **2018**, *140*, 13292–13300.

[23] Chen, M.; Luan, C. R.; Zhang, M.; Rowell, N.; Willis, M.; Zhang, C. C.; Wang, S. L.; Zhu, X. H.; Fan, H. S.; Huang, W. et al. Evolution of CdTe magic-size clusters with single absorption doublet assisted by adding small molecules during prenucleation. *J. Phys. Chem. Lett.* **2020**, *11*, 2230–2240.

[24] Wang, Z.; Wang, T. H.; Zhang, C. C.; Zhang, M.; Chen, X. Q.; Fan, H. S.; Huang, W.; Luan, C. R.; Yu, K. Evolution of two types of ZnTe magic-size clusters displaying sharp doublets in optical absorption. *J. Phys. Chem. Lett.* **2021**, *12*, 4762–4768.

[25] He, Z. T.; Wang, D. Q.; Yu, Q. Y.; Zhang, M.; Wang, S. L.; Huang, W.; Luan, C. R.; Yu, K. Evolution of photoluminescent CdS magic-size clusters assisted by adding small molecules with carboxylic group. *ACS Omega* **2021**, *6*, 14458–14466.

[26] Liu, Y. Y.; Willis, M.; Rowell, N.; Luo, W. Z.; Fan, H. S.; Han, S.; Yu, K. Effect of small molecule additives in the prenucleation stage of semiconductor CdSe quantum dots. *J. Phys. Chem. Lett.* **2018**, *9*,

6356–6363.
[27] Abe, S.; Capek, R. K.; De Geyter, B.; Hens, Z. Reaction chemistry/nanocrystal property relations in the hot injection synthesis, the role of the solute solubility. *ACS Nano* **2013**, *7*, 943–949.
[28] Dai, Q. Q.; Kan, S. H.; Li, D. M.; Jiang, S.; Chen, H. Y.; Zhang, M. Z.; Gao, S. Y.; Nie, Y. G.; Lu, H. L.; Qu, Q. L. et al. Effect of ligands and growth temperature on the growth kinetics and crystal size of colloidal CdSe nanocrystals. *Mater. Lett.* **2006**, *60*, 2925–2928.
[29] Zhang, Q.; Zhang, A. Y.; Yang, P.; Shen, J. X. Synthesis of CdSe quantum dots using various long-chain fatty acids and their phase transfer. *J. Nanosci. Nanotechnol.* **2013**, *13*, 4235–4241.
[30] Choi, H.; Ko, J. H.; Kim, Y. H.; Jeong, S. Steric-hindrance-driven shape transition in PbS quantum dots: Understanding size-dependent stability. *J. Am. Chem. Soc.* **2013**, *135*, 5278–5281.
[31] Yu, W. W.; Peng, X. G. Formation of high-quality CdS and other II–VI semiconductor nanocrystals in noncoordinating solvents: Tunable reactivity of monomers. *Angew. Chem., Int. Ed.* **2002**, *41*, 2368–2371.
[32] Green, P. B.; Wang, Z. B.; Sohn, P.; Imperiale, C. J.; Voznyy, O.; Wilson, M. W. B. Glycol ether additives control the size of PbS nanocrystals at reaction completion. *J. Mater. Chem. C* **2020**, *8*, 12068–12074.
[33] Zhang, J.; Hao, X. Y.; Rowell, N.; Kreouzis, T.; Han, S.; Fan, H. S.; Zhang, C. C.; Hu, C. W.; Zhang, M.; Yu, K. Individual pathways in the formation of magic-size clusters and conventional quantum dots. *J. Phys. Chem. Lett.* **2018**, *9*, 3660–3666.
[34] Palencia, C.; Yu, K.; Boldt, K. The future of colloidal semiconductor magic-size clusters. *ACS Nano* **2020**, *14*, 1227–1235.
[35] Li, Y. ; Rowell, N. ; Luan, C. R. ; Zhang, M. ; Chen, X. Q. ; Yu, K. A two-pathway model for the evolution of colloidal compound semiconductor quantum dots and magic-size clusters. *Adv. Mater.* , in press,https://doi.org/10.1002/adma.202107940.
[36] Liu, M. Y.; Wang, K.; Wang, L. X.; Han, S.; Fan, H. S.; Rowell, N.; Ripmeester, J. A.; Renoud, R.; Bian, F. G.; Zeng, J. R. et al. Probing intermediates of the induction period prior to nucleation and growth of semiconductor quantum dots. *Nat. Commun.* **2017**, *8*, 15467.
[37] Zhu, T. T.; Zhang, B. W.; Zhang, J.; Lu, J.; Fan, H. S.; Rowell, N.; Ripmeester, J. A.; Han, S.; Yu, K. Two-step nucleation of CdS magic-size nanocluster MSC-311. *Chem. Mater.* **2017**, *29*, 5727–5735.
[38] Zhu, D. K.; Hui, J.; Rowell, N.; Liu, Y. Y.; Chen, Q. Y.; Steegemans, T.; Fan, H. S.; Zhang, M.; Yu, K. Interpreting the ultraviolet absorption in the spectrum of 415 nm bandgap CdSe magic-size clusters. *J. Phys. Chem. Lett.* **2018**, *9*, 2818–2824.
[39] Luan, C. R.; Gökçinar, Ö. Ö.; Rowell, N.; Kreouzis, T.; Han, S.; Zhang, M.; Fan, H. S.; Yu, K. Evolution of two types of CdTe magic-size clusters from a single induction period sample. *J. Phys. Chem. Lett.* **2018**, *9*, 5288–5295.
[40] He, L.; Luan, C. R.; Rowell, N.; Zhang, M.; Chen, X. Q.; Yu, K. Transformations among colloidal semiconductor magic-size clusters. *Acc. Chem. Res.* **2021**, *54*, 776–786.
[41] Zhao, M.; Chen, Q. Y.; Zhu, Y. C.; Liu Y. H.; Zhang, C. C.; Jiang, G.; Zhang, M.; Yu, K. Precursor compound enabled formation of aqueous-phase CdSe magic-size clusters at room temperature. *Nano Res.* **2022**, *15*, 2634–2642.
[42] LaMer, V. K.; Dinegar, R. H. Theory, production and mechanism of formation of monodispersed hydrosols. *J. Am. Chem. Soc.* **1950**, *72*, 4847–4854.
[43] García-Rodríguez, R.; Hendricks, M. P.; Cossairt, B. M.; Liu, H. T.; Owen, J. S. Conversion reactions of cadmium chalcogenide nanocrystal precursors. *Chem. Mater.* **2013**, *25*, 1233–1249.
[44] Thanh, N. T. K.; Maclean, N.; Mahiddine, S. Mechanisms of nucleation and growth of nanoparticles in solution. *Chem. Rev.* **2014**, *114*, 7610–7630.
[45] Bai, G. Y. ; Gao, D. ; Liu, Z. ; Zhou, X. ; Wang, J. J. Probing the critical nucleus size for ice formation with graphene oxide nanosheets. *Nature* **2019**, *576*, 437−441.
[46] Li, L. J.; Zhang, J.; Zhang, M.; Rowell, N.; Zhang, C. C.; Wang, S. L.; Lu, J.; Fan, H. S.; Huang, W.; Chen, X. Q. et al. Fragmentation of magic-size cluster precursor compounds into ultrasmall CdS quantum dots with enhanced particle yield at low temperatures. *Angew. Chem., Int. Ed.* **2020**, *59*, 12013–12021.
[47] Service, R. F. How far can we push chemical self-assembly. *Science* **2005**, *309*, 95.
[48] Busatto, S. ; de Mello Donega, C. Magic-size semiconductor nanostructures: Where does the magic come from? *ACS Mater. Au*, in press,DOI: 10.1021/acsmaterialsau.1c00075.
[49] Ithurria, S.; Dubertret, B. Quasi 2D colloidal CdSe platelets with thicknesses controlled at the atomic level. *J. Am. Chem. Soc.* **2008**, *130*, 16504–16505.
[50] Cossairt, B. M.; Owen, J. S. CdSe clusters: At the interface of small molecules and quantum dots. *Chem. Mater.* **2011**, *23*, 3114–3119.
[51] Riedinger, A.; Ott, F. D.; Mule, A.; Mazzotti, S.; Knüsel, P. N.; Kress, S. J. P.; Prins, F.; Erwin, S. C.; Norris, D. J. An intrinsic growth instability in isotropic materials leads to quasi-two-dimensional nanoplatelets. *Nat. Mater.* **2017**, *16*, 743–748.
[52] Pun, A. B.; Mazzotti, S.; Mule, A. S.; Norris, D. J. Understanding discrete growth in semiconductor nanocrystals: Nanoplatelets and magic-sized clusters. *Acc. Chem. Res.* **2021**, *54*, 1545–1554.
[53] Zhu, J. M.; Cao, Z. P.; Zhu, Y. C.; Rowell, N.; Li, Y.; Wang, S. L.; Zhang, C. C.; Jiang, G.; Zhang, M.; Zeng, J. R. et al. Transformation pathway from CdSe magic-size clusters with absorption doublets at 373/393 nm to clusters at 434/460 nm. *Angew. Chem., Int. Ed.* **2021**, *60*, 20358–20365.
[54] Prins, P. T.; Montanarella, F.; Dümbgen, K.; Justo, Y.; van der Bok, J. C.; Hinterding, S. O. M.; Geuchies, J. J.; Maes, J.; De Nolf, K.; Deelen, S. et al. Extended nucleation and superfocusing in colloidal semiconductor nanocrystal synthesis. *Nano Lett.* **2021**, *21*, 2487–2496.
[55] Liu, Y. Y.; Rowell, N.; Willis, M.; Zhang, M.; Wang, S. L.; Fan, H. S.; Huang, W.; Chen, X. Q.; Yu, K. Photoluminescent colloidal nanohelices self-assembled from CdSe magic-size clusters via nanoplatelets. *J. Phys. Chem. Lett.* **2019**, *10*, 2794–2801.
[56] Yu, K.; Ouyang, J. Y.; Zaman, M. B.; Johnston, D.; Yan, F. J.; Li, G.; Ratcliffe, C. I.; Leek, D. M.; Wu, X. H.; Stupak, J. et al. Single-sized CdSe nanocrystals with bandgap photoemission via a noninjection one-pot approach. *J. Phys. Chem. C* **2009**, *113*, 3390–3401.
[57] Calvin, J. J.; Brewer, A. S.; Alivisatos, A. P. The role of organic ligand shell structures in colloidal nanocrystal synthesis. *Nat. Synth.* **2022**, *1*, 127–137.
[58] Ouyang, J. Y.; Zaman, M. B.; Yan, F. J.; Johnston, D.; Li, G.; Wu, X. H.; Leek, D.; Ratcliffe, C. I.; Ripmeester, J. A.; Yu, K. Multiple families of magic-sized CdSe nanocrystals with strong bandgap photoluminescence via noninjection one-pot syntheses. *J. Phys. Chem. C* **2008**, *112*, 13805–13811.
[59] Ghosh, S.; Ray, A.; Pramanik, N. Self-assembly of surfactants: An overview on general aspects of amphiphiles. *Biophys. Chem.* **2020**, *265*, 106429.
[60] Zhang, J. ; Li, L. J. ; Rowell, N. ; Kreouzis, T. ; Willis, M. ; Fan, H. S. ; Zhang, C. C. ; Huang, W. ; Zhang, M. ; Yu, K. One-step approach to single-ensemble CdS magic-size clusters with enhanced production yields. *J. Phys. Chem. Lett.* **2019**, *10*, 2725−2732.
[61] Liu, S. P.; Yu, Q. Y.; Zhang, C. C.; Zhang, M.; Rowell, N.; Fan, H. S.; Huang, W.; Yu, K.; Liang, B. Transformation of ZnS precursor compounds to magic-size clusters exhibiting optical absorption peaking at 269 nm. *J. Phys. Chem. Lett.* **2020**, *11*, 75–82.
[62] Van Embden, J.; Mulvaney, P. Nucleation and growth of CdSe nanocrystals in a binary ligand system. *Langmuir* **2005**, *21*, 10226–10233.